THIN FILM POLYCRYSTALLINE SILICON SOLAR CELLS

Quarterly Technical Progress Report No. 3 for Period April 1—June 30, 1980

By
K. R. Sarma
M. J. Rice
R. Legge
R. J. Ellis

June 1980

Motorola, Inc.
Phoenix, Arizona

U.S. Department of Energy

Solar Energy

DISCLAIMER

This report was prepared as an account of work sponsored by an agency of the United States Government. Neither the United States Government nor any agency Thereof, nor any of their employees, makes any warranty, express or implied, or assumes any legal liability or responsibility for the accuracy, completeness, or usefulness of any information, apparatus, product, or process disclosed, or represents that its use would not infringe privately owned rights. Reference herein to any specific commercial product, process, or service by trade name, trademark, manufacturer, or otherwise does not necessarily constitute or imply its endorsement, recommendation, or favoring by the United States Government or any agency thereof. The views and opinions of authors expressed herein do not necessarily state or reflect those of the United States Government or any agency thereof.

DISCLAIMER

Portions of this document may be illegible in electronic image products. Images are produced from the best available original document.

DISCLAIMER

THIN FILM POLYCRYSTALLINE SILICON SOLAR CELLS

QUARTERLY TECHNICAL PROGRESS REPORT NO. 3
FOR PERIOD
1 APRIL 1980 - 30 JUNE 1980

K.R. SARMA, M.J. RICE, R. LEGGE, R.J. ELLIS

JUNE 1980

MOTOROLA, INC.
5005 EAST MCDOWELL ROAD
PHOENIX, ARIZONA 85008

UNITED STATES
DEPARTMENT OF ENERGY
DIVISION OF SOLAR TECHNOLOGY
AND
SOLAR ENERGY RESEARCH INSTITUTE
UNDER DOE SUBCONTRACT NO. XS-9-8277-1

MOTOROLA PROJECT NO. 2377

PREFACE

This Quarterly Report No. 3, covering the period April 1, 1980 to June 30, 1980, was prepared by the Solar Energy R&D Department, I. A. Lesk, Manager, Motorola Inc., Phoenix, Arizona 85008. This report describes the work performed under SERI Contract No. XS-9-8277-1. K. R. Sarma is the prinicpal investigator. Others who participated in this program are R. W. Gurtler, M. J. Rice, R. N. Legge, R. J. Ellis and W. Salina.

ABSTRACT

During this third quarter of the program, the high pressure plasma (hpp) deposition process has been thoroughly evaluated using $SiHCl_3$ and $SiCl_4$ silicon source gases, by the gas chromatographic analysis of the effluent gases from the reactor. Both the deposition efficiency and reactor throughput rate were found to be consistently higher for hpp mode of operation compared to conventional CVD mode. The figure of merit for various chlorosilanes as a silicon source gas for hpp deposition is discussed. A new continuous silicon film deposition scheme is developed, and system design is initiated. This new system employs gas interlocks and eliminates the need for gas curtains which have been found to be problematic. Solar cells (2 cm x 2 cm area) with AM1 efficiencies of up to 12% were fabricated on RTR grain enhanced hpp deposited films. The parameters of a 12% cell under simulated AM1 illumination were: V_{OC} = 0.582 volts, J_{SC} = 28.3 mA/cm^2 and F.F. = 73.0%.

TABLE OF CONTENTS

LIST OF FIGURES

LIST OF TABLES

1.0 INTRODUCTION

The objectives of this research program are: a) investigation of a semi-continuous plasma deposition system as a means for efficient, high rate deposition of polycrystalline silicon films, b) development of low-cost reuseable substrates for deposition and shear separation of the silicon films, c) optimization and subsequent grain enhancement of the films through laser RTR recrystallization, and d) demonstration of at least 12% efficient, large area (greater than 10 cm^2) solar cells fabricated on grain-enhanced silicon films.

During this quarter, we have characterized the plasma depositon process using SiHCl$_3$ and SiCl$_4$ as the silicon source gases gy gas chromatographic analysis of the reactor effluent gases. Deposition efficiencies were determined as a function of chlorosilane concentration and substrate temperature. Comparisons were made in the deposition reactor performance between the CVD and plasma deposition modes under otherwise identical conditions. Under practical silicon film deposition conditions, deposition efficiencies and silicon film throughput rates were found to be consistently higher with the plasma deposition mode of operation compared to the CVD mode. The observed results are discussed and explained qualitatively from thermodynamic, kinetic and mass transport considerations.

A new continuous silicon film deposition scheme has been developed. This new scheme employs gas interlocks and eliminates the requirement for gas seals used in the present semicontinuous system and which are found to be problematic.

A series of experiments has been performed in the grain enhancement and solar cell fabrication areas aimed at determining the factors limiting the performance of solar cells fabricated on RTR grain enhanced plasma deposited silicon films. The results of these experiments suggest that the detrimental chemical impurities in these films are at an inconsequential level, and it is the

1

presence of defects (primarily dislocations) which are currently limiting

the performance of the solar cells. However, in the latest batch of

solar cells fabricated on RTR grain enhanced plasma deposited films, we have

observed AM1 conversion efficiencies of up to 12% on 4 cm^2 area cells.

2.0   CHARACTERIZATION OF PLASMA DEPOSITION PROCESS

We have continued characterization of the high pressure plasma (hpp) deposition process with various experimental parameters including the type of silicon bearing gas used, reactant concentration, total reactant flow rate, and substrate temperature during deposition. Experiments aimed at comparing the silicon deposition process under HPP and conventional CVD modes were also performed. Gas chromatography has been used to evauate each silicon deposition process; details of the gas chromatographic procedures were described earlier (1,2,). The silicon deposition process is characterized by determining the efficiency of silicon deposition; the error in deposition efficiency determined by gas chromatographic analysis is estimated to be within ±0.5%.

In the following we present the experimental results and explain them on a qualitative basis using thermodynamic, kinetic and mass transport considerations. We also discuss the suitability of various chlorosilanes as silicon source gases in the hpp deposition process.

2.1   EXPERIMENTAL RESULTS

Table 1 summarizes the results, obtained using $SiHCl_3$ as the silicon source gass. Figure 1 shows the effect of chlorosilane concentration on deposition efficiency when the substrate temperature and total reactant flow rate are kept constant at $1100^{\circ}C$ and 30 LHM respectively. From the reactor dimensions (5 cm x 5 cm x 60 cm), the flow velocity and residence time can be calculated to be 20 cm/sec. and 3 sec. respectively. Renolds number calculations for all the reactant flows employed indicated that the flow will be in the turbulent regime. Also diffusion length calculations for the heaviest molecule ($SiCl_4$) in the reactor system using the diffusion coefficient (6.3 cm^2/sec) (3) and residence

TABLE 1

SUMMARY OF RESULTS OBTAINED USING SiHCl$_3$ AS SILICON SOURCE GAS.

T ($^{\circ}$C)	MODE	FLOW (LPM)	DEPOSITION EFFICIENCY		
			Cl/H = .04	Cl/H = 0.08	Cl/H = 0.1
1050	CVD	15	40.5	30.9	26.5
	HPP	15	49.3	35.6	29.8
	CVD	30	39.0	25.0	21.7
	HPP	30	53.5	35.1	32.7
1100	CVD	15	47.3	35.7	32.3
	HPP	15	54.3	38.5	33.5
	CVD	30	52.2	36.1	31.5
	HPP	30	55.1	37.9	34.0
1150	CVD	15	51.9	34.2	30.7
	HPP	15	49.3	35.6	32.3
	CVD	30	53.9	31.7	27.8
	HPP	30	55.7	35.8	31.7
1200	CVD	15	48.0	34.9	30.5
	HPP	15	49.8	37.3	33.2
	CVD	30	51.6	31.4	29.0
	HPP	30	68.4	39.0	
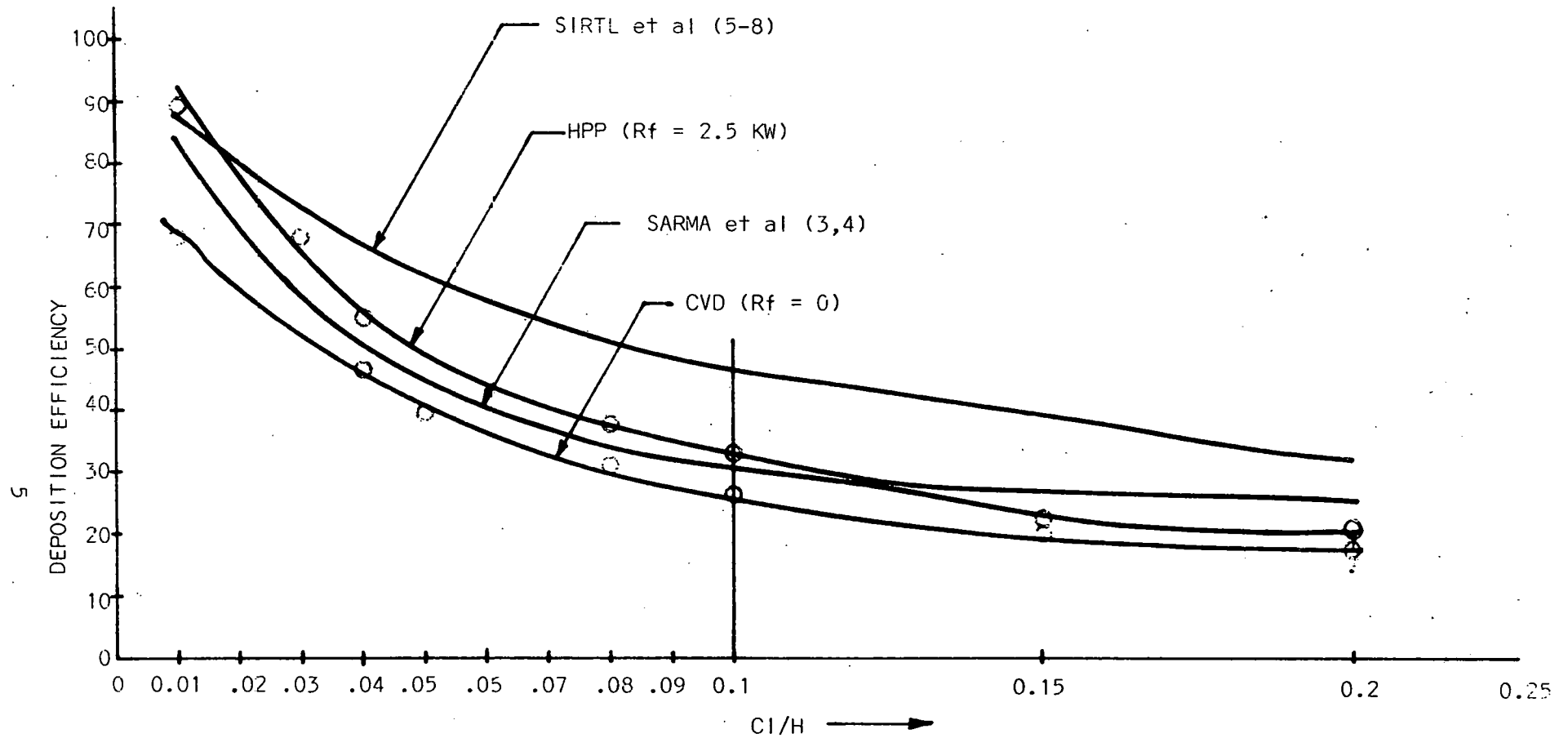
FIGURE 1: DEPOSITION EFFICIENCY USING SiHCl₃ AS THE SILICON-BEARING GAS
(TOTAL REACTANT GAS FLOW RATE = 30 LPM: SUBSTRATE TEMPERTURE = 1100°C).

5

time (3 sec.) indicated that it is approximately the same as the reactor cross sectional size. From these considerations, good gas mixing can be expected in the reactor system. Along with the experimental data under CVD and HPP conditions, data from theoretical calculations by Sirtl and Sarma are also shown in Figure 1. (The two theoretical curves presented in Figure 1 will be discussed later in this section).

As can be seen in Figure 1, observed deposition efficiency is higher for the HPP mode than for the corresponding CVD mode. Also, in the HPP mode, observed efficiency is higher than predicted by thermodynamic equilibrium calculations (4,5) (Sarma) for Cl/H < 0.1. For Cl/H > 0.1 the HPP efficiencies are lower than calculated equilibrium values. Observed CVD efficiencies are consistently lower than calculated equilibrium values. In some experiments performed with exceedingly small reactant flow rates (high residence times) to assure equilibrium, the CVD efficiencies approached the equilibrium efficiencies more closely, but were never found to exceed the equilibrium values predicted from our calculations.

Of the two theoretical curves presented in Figure 1, one is obtained from our work (4,5) and one from Sirtl et al. publications (6-8). As can be seen in Figure 1, while the two theoretical curves are in qualitative agreement regarding the variation of deposition efficiency with concentration, they differ quantitatively. Sirtl's calculations predict much higher deposition efficiencies than ours. Sirtl's calculations (6-8) were available when we started work on this contract. Hence, our calculations were aimed at extending Sirtl's calculations to the conditions pertaining the HPP deposition (plasma temperatures up to 5000K). Thus, we employed the same calculation technique as Sirtl et al. (free energy minimization technique) for calculating the chemical thermodynamic equilibrium. We have not yet clearly identified the reasons for disagreement between the two calculation results. However, it should be

pointed out that Sirtl et al. used the thermodynamic data available in the year 1972, and we have used data from JANAF tables (9) in the year 1978. JANAF tables are regularly updated with more acceptable thermodynamic data. Hence, it is possible that the difference between the two may be associated with the thermodynamic data used and the species considered. We plan to investigate this further. It is worth pointing out that we were not able to locate any experimental work in the literature in which the silicon deposition efficiency (using $SiHCl_3$ as the silicon source gas) appraoched the equilibrium value predicted by Sirtl et al. calculations.

Table 2 summarizes the results obtained using $SiCl_4$ as a source gas. Figure 2 shows the effect of chlorosilane concentration on the deposition efficiency. $SiCl_4$ source gas deposition differs from $SiHCl_3$; in particular, etching reactions become important with $SiCl_4$ at fairly low reactant concentrations. As can be seen in Figure 2, HPP efficiencies are higher than CVD efficiencies over most of the concentration range. For Cl/H > 0.15, CVD efficiency appears to be slightly higher than the HPP value. While the difference between the two (~ 1.0% for Cl/H = 0.2) appears to be comparable to the accuracy of the measurement, it is found to be real as inferred from the result of a number of repetitions of this experiment. Further it can be seen from Figure 2 that the experimental efficiencies are higher than our predicted equilibrium values and lower than those of Sirtl et al. Also our calculations predict etching for Cl/H $\simeq$ 0.125 and Sirtl et. al. predict etching for Cl/H $\simeq$ 0.3; experimentally, etching has not been observed for Cl/H ratios of up to 0.3.

Figure 3 shows the effect of substrate temperature during deposition on the efficiency. This figure shows data for two different concentrations, Cl/H = 0.08 and 0.1, when using $SiHCl_3$ as the silicon source gas. The maximum in deposition

7

TABLE 2

SUMMARY OF RESULTS OBTAINED USING $SiCl_4$ AS SILICON SOURCE GAS

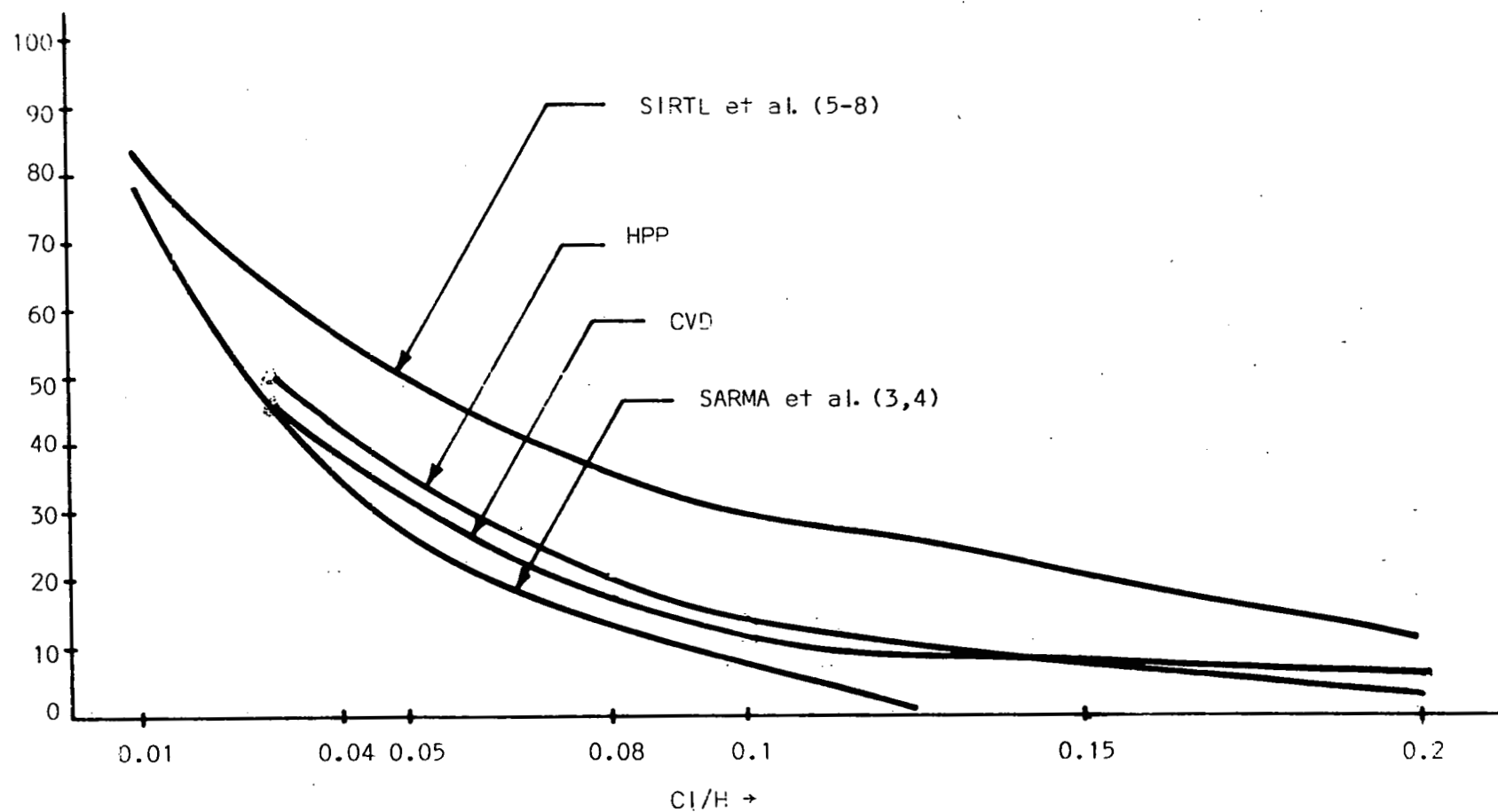| T (^{o}C)	MODE	FLOW	DEPOSITION EFFICIENCY		
			Cl/H = 0.04	Cl/H = 0.08	Cl/H = 0.1
1050	CVD	15	43.6	18.8	11.9
	HPP	15	41.8	18.1	10.6
	CVD	30	33.8	13.9	10.1
	HPP	30	42.6	14.4	9.5
1100	CVD	15	40.9	19.2	12.9
	HPP	15	43.1	19.2	11.9
	CVD	30	46.0	17.7	12.8
	HPP	30	50.0	17.2	11.5
1150	CVD	15	54.0	20.3	13.0
	HPP	15	54.4	19.6	11.8
	CVD	30	50.8	19.6	13.7
	HPP	30	55.1	19.3	11.5
1200	CVD	15			
	HPP	15			
	CVD	30			
	HPP	30			

FIGURE 2: DEPOSITION EFFICINECY USING SiCl$_4$ AS THE SILICON BEARING GAS
(TOTAL REACTANT FLOW RATE = 30 LPM, SUBSTRATE TEMPERATURE = 1100°C)
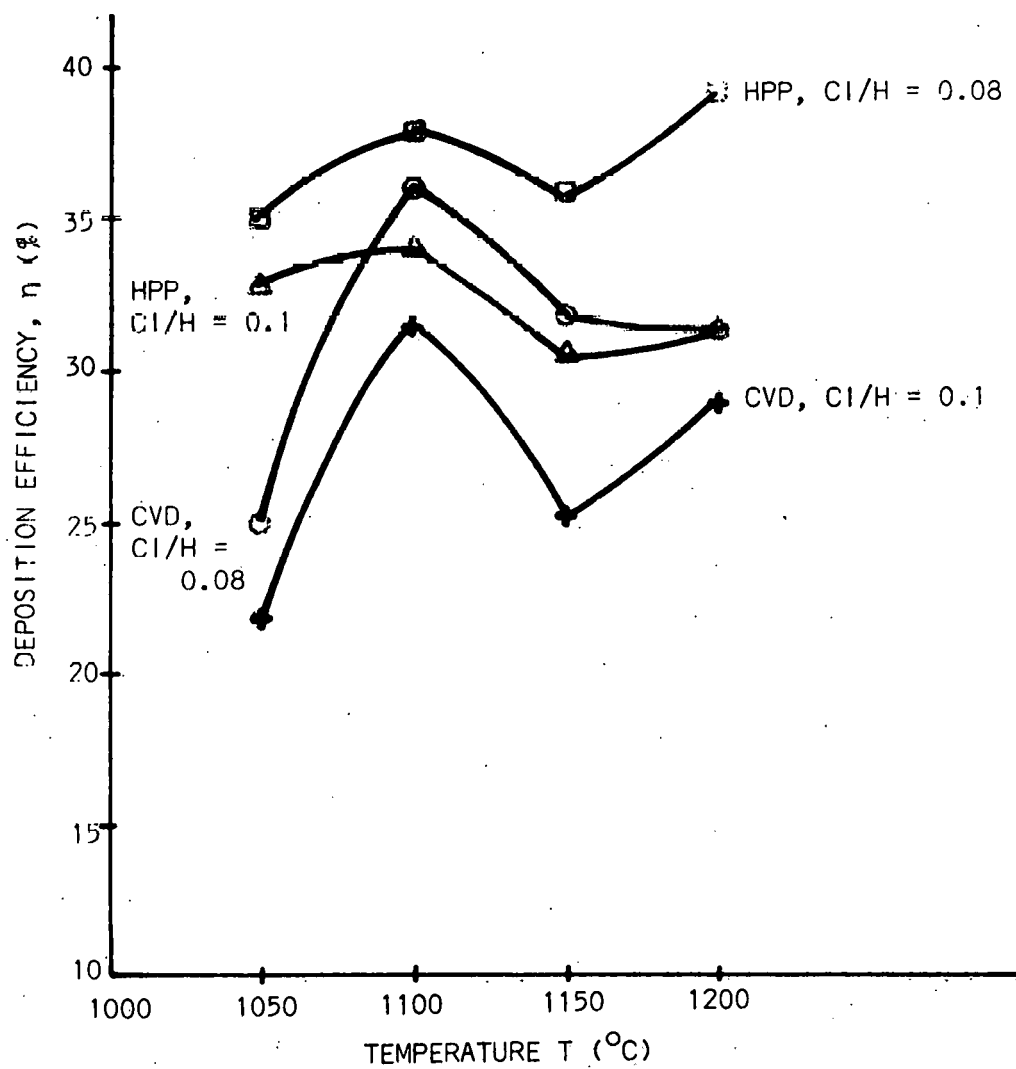
FIGURE 3: DEPOSITION EFFICIENCY VS. SUBSTRATE TEMPERATURE
USING $SiHCl_3$ AS SILICON SOURCE GAS. (TOTAL
REACTANT FLOW RATE = 30 LPM).

efficiency at around 1100°C is in qualitative agreement with Sirtl et al. equilibrium calculations. (Our calculations do not include low temperatures and hence comparisons could not be made.) Figure 3 indicates that the HPP efficiencies are consistantly higher than CVD efficiencies.

Figure 4 shows reactor throughput (given in terms of a constant times the grams of silicon deposited per minute) calculated from data in Figures 1 and 2. Reactor throughput is an important parameter since it determines the number of reactors (capital) required for a given capacity which in turn determines production floor space requirements. As seen in Figure 4, when using $SiCl_4$ as the silicon source gas, a maximum in throughput occurs at a concentration, Cl/H, of about 0.05. Using $SiHCl_3$ as the silicon source gas, throughput increases continuously with concentration. However, for higher concentrations, silicon powder formation due to excessive gas phase nucleation becomes a severe problem. Thus the onset of powder formation sets an upper limit to the concentration (Cl/H ratio) that can be employed and the reactor throughput achieved. This concentration limit is found to be around a Cl/H ratio of 0.1. This concentration limit is found to be somewhat higher for CVD compared to HPP deposition. Thus from figure 4 it can be seen that, comparing $SiCl_4$ and $SiHCl_3$ as a silicon source gas, reactor throughput is higher in the HPP mode than in the CVD mode under practical silicon deposition conditions. Also, the practical reactor throughput is about a factor of two higher for $SiHCl_3$ compared to a $SiCl_4$ source.

2.2   DISCUSSION

2.2.1   THERMODYNAMIC FACTORS

While, in general, practical silicon deposition reactors do not operate under

FIGURE 4: REACTOR THROUGHPUT AS A FUNCTION OF CONCENTRATION.

equilibrium conditions, consideration of thermodynamic equilibrium helps one
to predict the range of performance that can be expected. For example, by
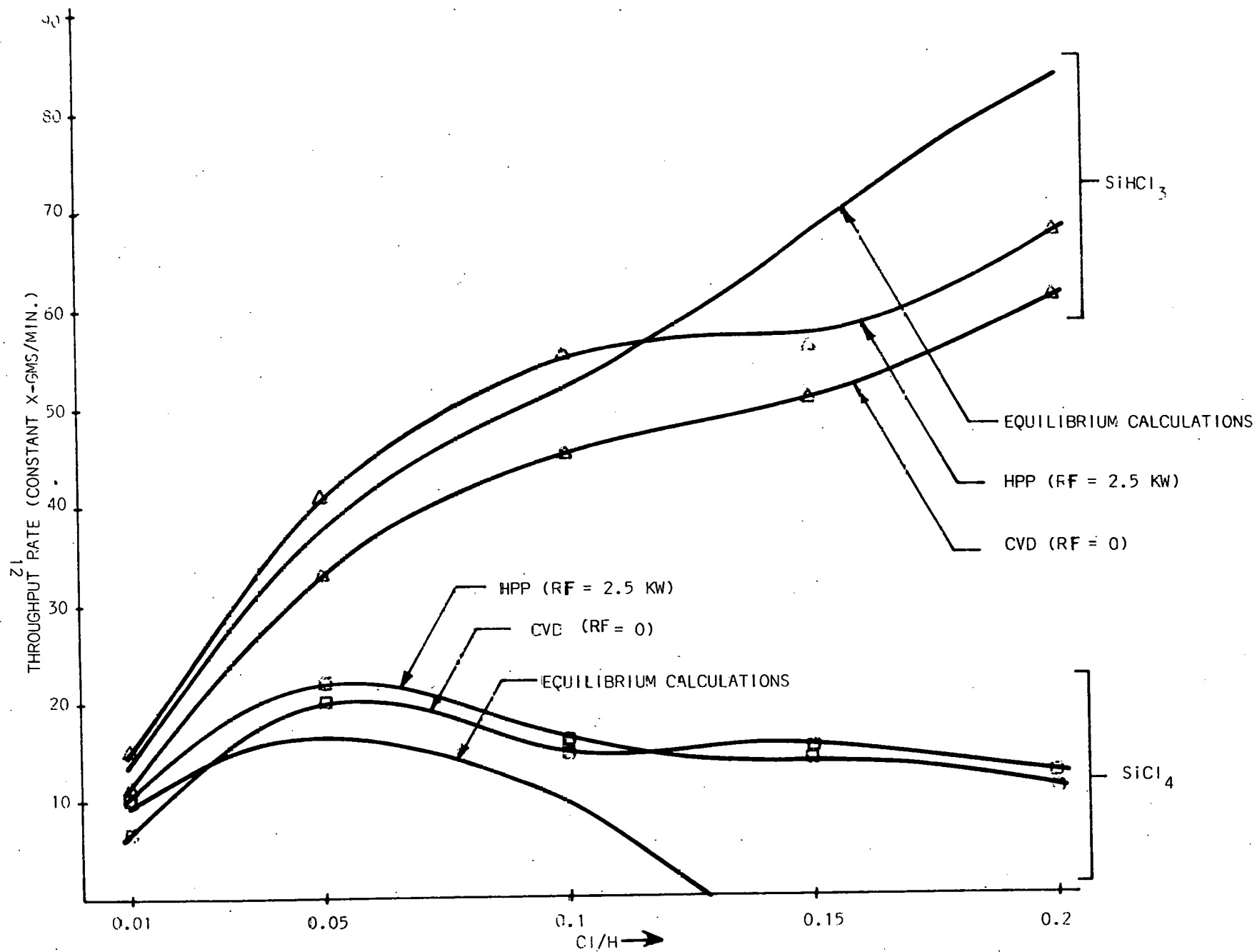examining the results of equilibrium calculations (4,5) such as those in Figure 5,
one can easily predict the relative performance of various chlorosilanes in a
deposition reactor. Figure 5 shows the equilibrium deposition efficiencies for
SiH_2Cl_2, $SiHCl_3$ and $SiCl_4$ sources as a function of concentration for a
substrate temperature of $1100^{\circ}C$ and reactor pressure of 1 atm. Experimental
deposition efficiencies are in qualitative agreement with the results of
equilibrium calculation: i.e., deposition efficiencies are the highest for
SiH_2Cl_2 and lowest for $SiCl_4$, and deposition efficiency decreases for all these
chlorosilanes with increasing concentration.

Similarly effect of substrate temperature can be examined from the
equilibrium digaram shown in Figure 6. In this figure, $\frac{Si}{Cl}$ ratio in the gas
phase in equilibrium is plotted as a function of concentration (Cl/H ratio)
of the reactor input gas stream for various temperatures. Using Figure 6, the
deposition efficiency, η, can be calculated using the equation

$$\eta = \frac{\left.\frac{Si}{Cl}\right)_{input} - \left.\frac{Si}{Cl}\right)_{eqbm.}}{\left.\frac{Si}{Cl}\right)_{input}} \times 100$$

where $Si/Cl)_{input}$ is determined by the chlorosilane source used. For example
for SiH_2Cl_2, $Si/Cl)_{input} = 0.5$ and for $SiCl_4$, $Si/Cl)_{input} = 0.25$.

Thus from the above expression we can see that for a given source,
efficiency will be higher when $Si/Cl)_{eqbm.}$ is lower. In Figure 6 we have used
Sirtl et al. data (6-8) for low temperatures (T≤1700K) and our calculated data (4,5)
for high temperatures (T>1700K). Since we use this figure only to explain trends in
silicon deposition, quantitative disagreement between the two sets of data is
not of concern. From Figure 6, it can be seen that $Si/Cl)_{eqbm.}$ increases with
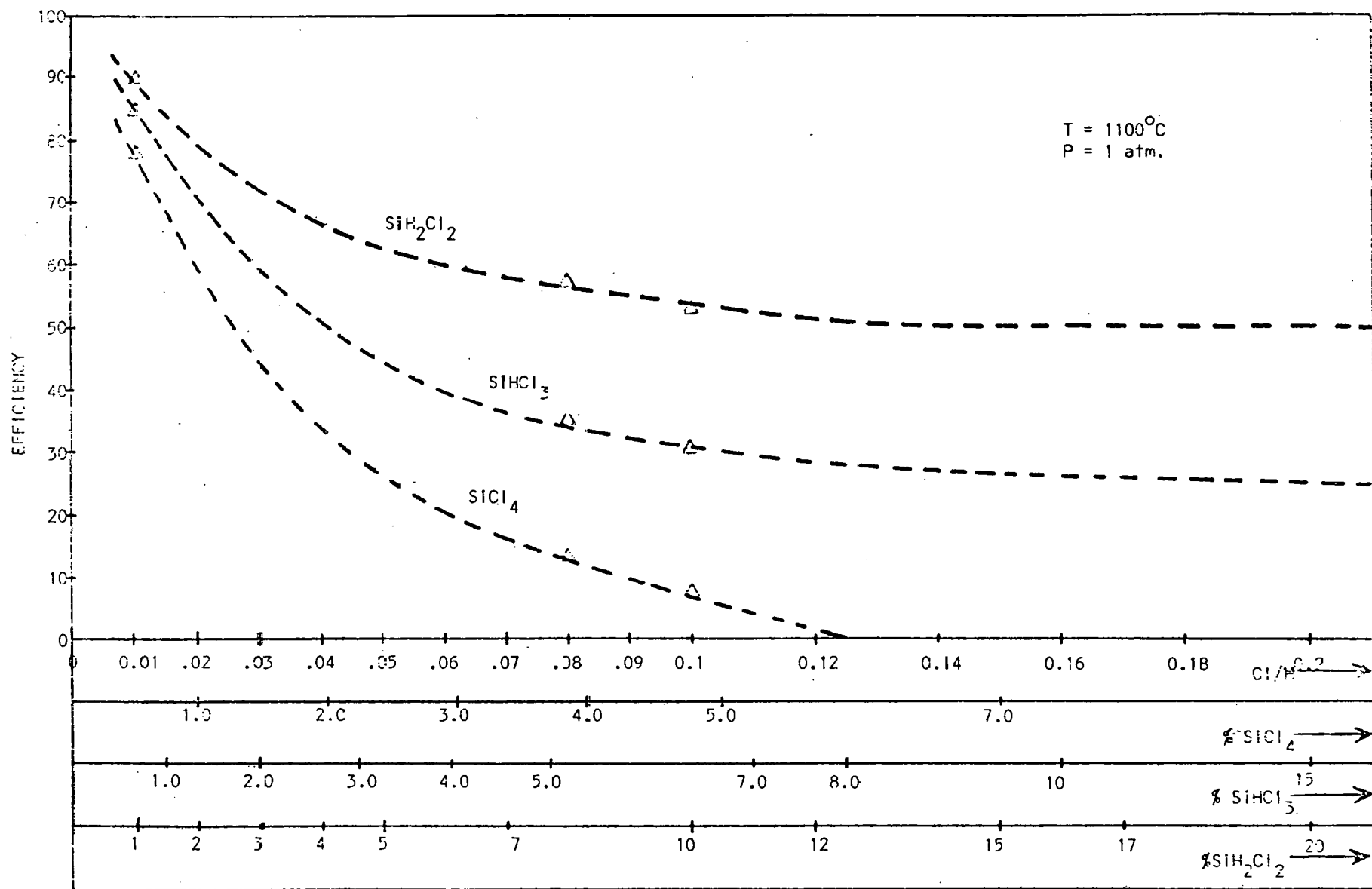
FIGURE 5: EQUILIBRIUM DEPOSITION EFFICIENCY AS A FUNCTION OF CONCENTRATION WITH DIFFERENT CHLOROSILANE SOURCES FOR $T = 1100^{\circ}C$ and $P = 1$ atm.
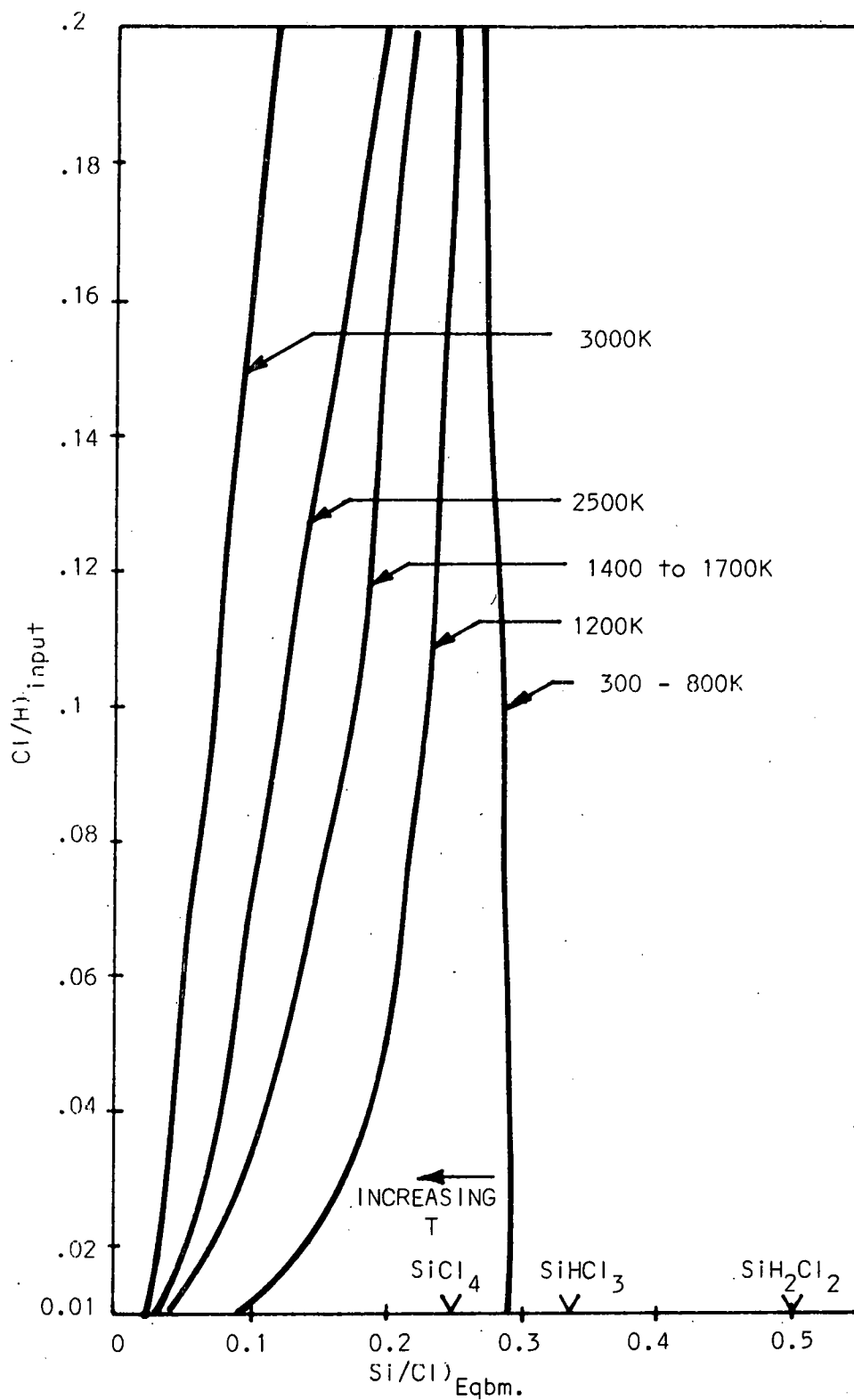
FIGURE 6: Si-Cl-H EQUILIBRIUM DIAGRAM GENERATED FROM THE DATA IN REFERENCES (4 - 8).

increasing temperature, levels off at around 1400 - 1700K and then increases again. Thus, efficiency increases with increasing temperature, then levels off between 1400 - 1700K and then increases further with temperature.

In a conventional CVD process, reactant gas temperature rises from room temperature to the substrate temperature, and never exceeds the substrate temperature. Thus the approach to equilibrium is from right to left in Figure 6 (low temperature to high temperature). Unless sufficient residence time is allowed, equilibrium (thermal and chemical) will not be reached. In the case of high pressure plasma deposition, the reactant gases experience very high temperatures (4) (~4000K) in the plasma beam and then are quenched to the substrate temperature. Compositional equilibrium can be assumed in this high temperature, high pressure plasma. (At this time, it should be pointed out that above the boiling point of silicon, all components of the system will be in vapor phase, and the $Si/Cl)_{eqbm}$ in Figure 6 is obtained by considering the silicon species containing Cl and/or H). As the plasma is quenched to the substrate temperature, equilibrium is approached from the left of Figure 6 to right. By rapidly quenching the high temperature equilibrium, it should be possible to obtain higher deposition efficiencies with HPP compared to CVD. This has been the rationale for investigating HPP as a means for economically depositing microcrystalline silicon films. From the experimental results, it can be seen that while the improvements in efficiencies are not as much as we thought possible, useful improvement in efficiency was indeed obtained. In the next sections we will examine the other considerations that determine the efficiency improvements obtainable with HPP silicon deposition.

2.2.2 SILICON DEPOSITION MECHANISMS

In the case of convention cold wall CVD reactors; the deposition mechanism generally involves, transport of reactants to the substrate surface, chemical reaction on the surface producing silicon atoms, and incorporation of these atoms into the growing silicon film, as shown in Figure 7. However, a second deposition mode involves occurrence of chemical reactions in the gas phase producing free silicon atoms, condensation of these atoms into nuclei in the gas phase, transport of these nuclei to the substrate surface and their incorporation into the growing silicon film. This latter mode of deposition becomes important in CVD reactors with the use of SiH_2Cl_2 and SiH_4 source gases, higher substrate temperatures, and hot wall deposition systems (10-12).

With HPP deposition, however, the gas phase nucleation and deposition mode is found to be important under all conditions regardless of the type of chlorosilane, its concentration, and the reactor (substrate) temperature employed. One of the consequences of gas phase nucleation can be powder growth, i.e. silicon nuclei, instead of reaching the substrate surface and contributing to film growth, grow in the vapor phase to a larger size and then deposit in the form of a powder. This powder formation constitutes a loss process, and furthermore creates problems in the exhaust gas (chlorosilane and hydrogen) recovery system. While it has not been, so far, possible to estimate the relative contributions of these two different deposition mechanisms in the HPP deposition process, to film deposition rates, powder formation is found to be at an inconsequential level in the horizontal operation of the system under practical film growth conditions. The reasons for this will be discussed under Section 2.4.4 (transport effects). Figure 8 schematically illustrates the deposition model in the HPP reactor.

17
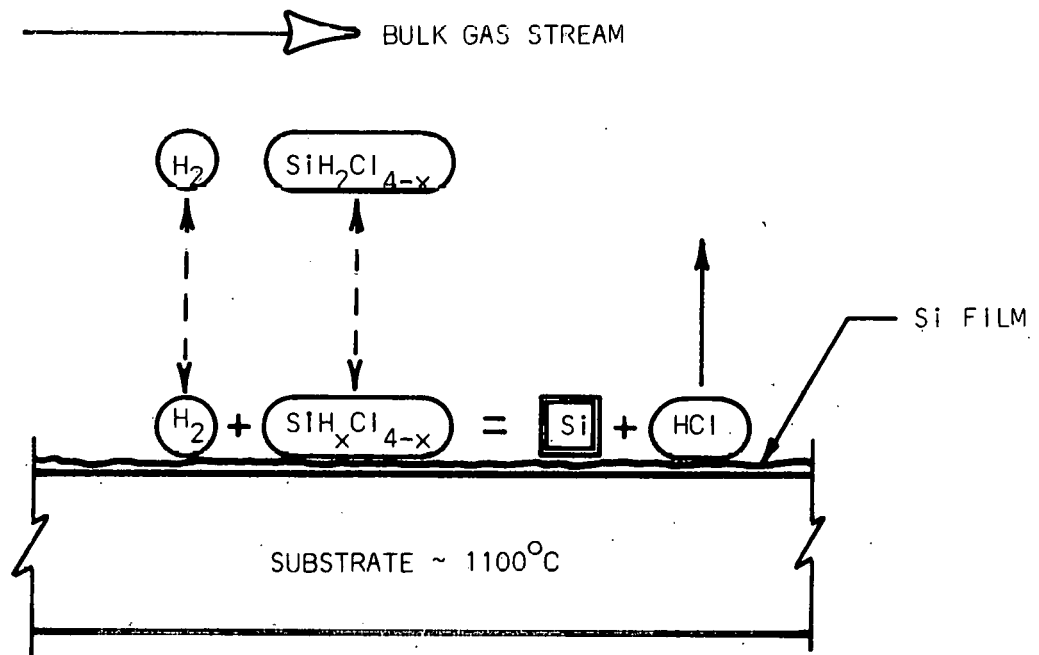
FIGURE 7: SCHEMATIC ILLUSTRATION OF THE SILICON DEPOSITION MECHANISM IN A CONVENTIONAL COLD WALL CVD REACTOR.

QUARTZ DEPOSITION CHAMBER

MOLYBDENUM TESS SUBSTRATE (~1100°C)

DEPOSITING SILICON FILM

$H_2 + SiH_xCl_{4-x}$

~4000°C

Mixture of gas species containing the elements Si, H and Cl and small silicon particles at high temperature.

HPP BEAM

HPP NOZZLE

FICK AND SORET DIFFUSION OF GAS SPECIES AND SILICON PARTICLES

FIGURE 8:   SCHEMATIC ILLUSTRATION OF THE HPP DEPOSITION MODEL.   SORET DIFFUSION IS EXPECTED TO BE IMPORTANT ONLY IN THE INITIAL REGION OF THE DEPOSITION REACTOR.

19

2.2.3   KINETIC EFFECTS

As discussed previously, kinetic factors determine the deposition efficiency achievable in the HPP process. Figure 9 shows equilibrium concentrations (4,5) of the species present in the HPP deposition reactor. Assuming that chemical equilibrium is attained in the high temperature (~4300K) plasma beam, the predominant species will be H, Cl, Si (g), H_2 and HCl. As the temperature is lowered through the boiling point of silicon (~2950), there will be a driving force for condensation of silicon vapor, and upon further cooling through the melting temperature (~1683K) there will be a driving force for solidification of silicon. At the same time as the temperature is lowered, there is a tendency for formation of $SiCl_2$ and $SiCl_3$ species. However, silicon condensation could occur before the equilibrium $SiCl_2$ species concentration increases. When this happens, the reaction between the condensed phase and chlorine will be the rate limiting step in the attainment equilibrium as the gas mixture is quenched. Another kinetic factor of importance is incorporation of gas phase nucleated silicon into the growing silicon film. This factor has not been found to be very important, probably because of the extremely small particle size (<<1μm), at least, in the horizontal operation of the HPP system (13). This sequence of events qualitatively explains the improvements in deposition efficiencies observed in the HPP deposition process.
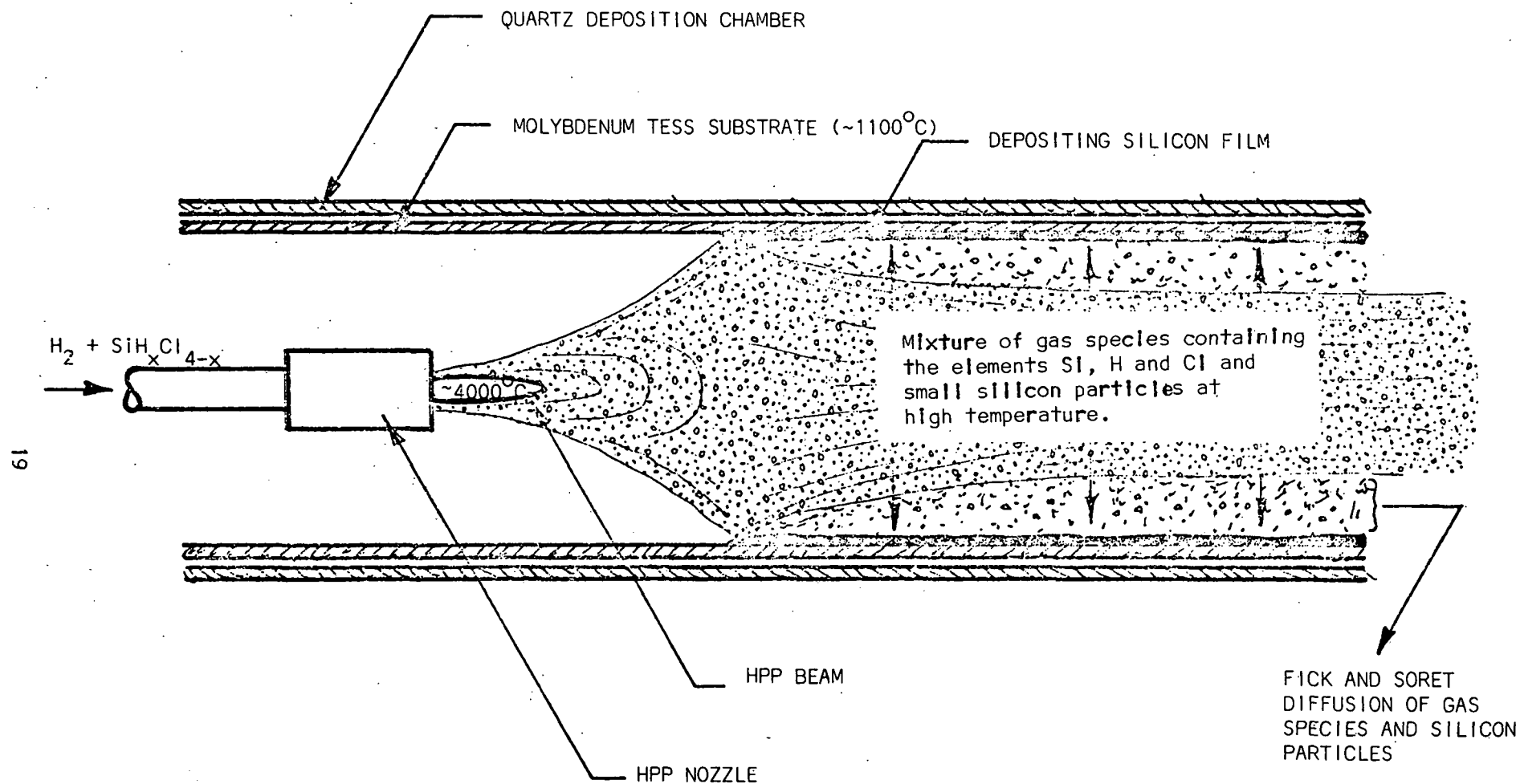
2.2.4   TRANSPORT EFFECTS

A complete discussion of the HPP deposition process has to include the various mass transport processes taking place in the deposition chamber. To develop an accurate mass transport model, chemical reactions occuring in the system
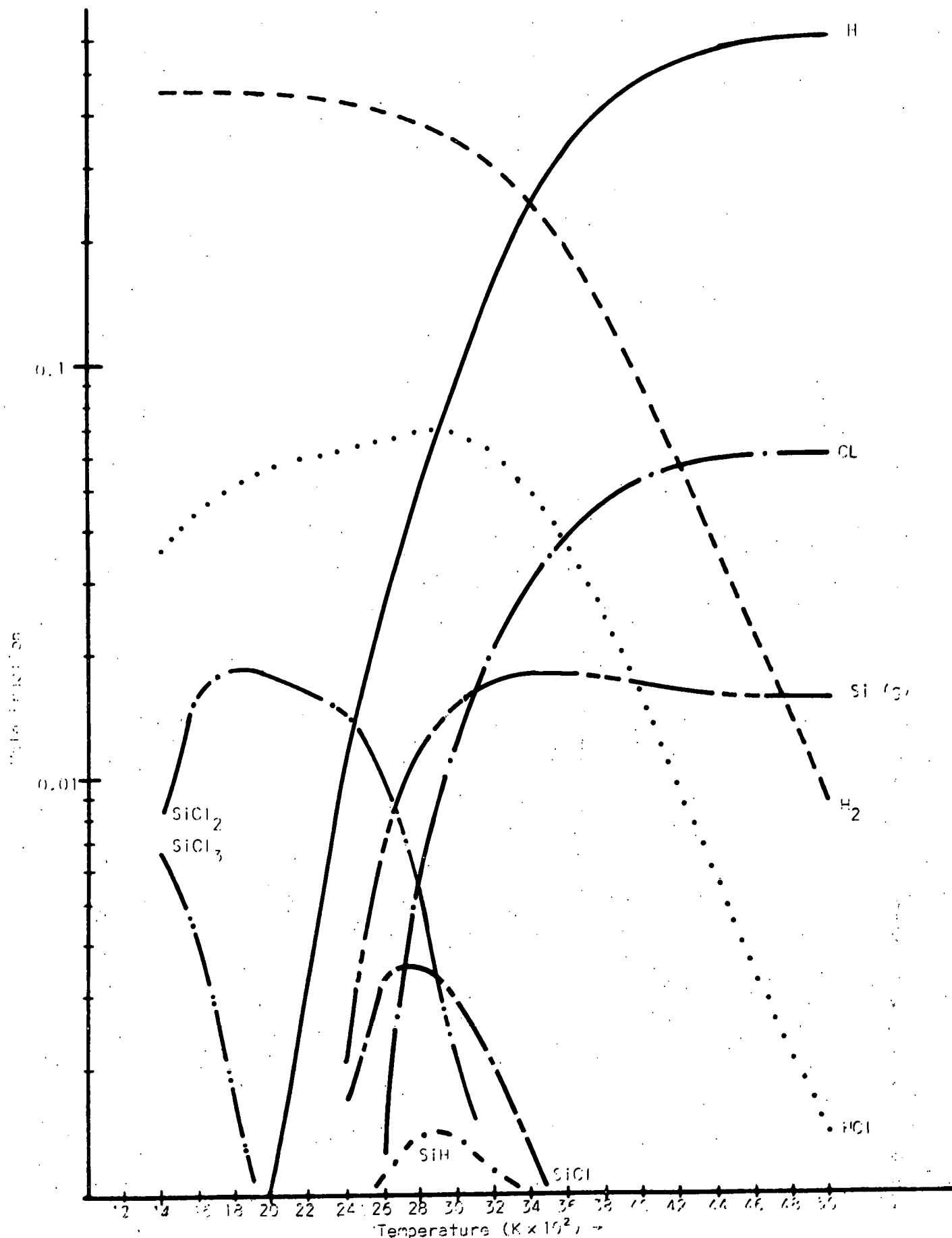
9. Relative concentrations of various species containing Si, H, Cl as a function of temperature for P=1 atm and Cl/H = 0.1. (Reference 12).

21

have to be considered simultaneously. Silicon deposition reactors involving
gas phase nucleation are currently being modelled by Aerochem Research
Laboratories, Inc. without taking into account the simultaneous chemical reactions
(see for example reference 14).

The transport of species in the HPP reactor takes place due to
convective and diffusive processes driven by both compositional
gradients (Fick) and thermal gradients (Soret). While the Fick diffusion
coefficient for all species is positive (i.e. diffusion down the concentration
gradient), the Soret diffusion coefficient will be negative for some species
(i.e., in a temperature gradient lighter species tend to move towards high
temperatures and heavier species towards low temperatures). Steep radial
temperature gradients exist in the beginning part of the HPP reactor where the
plasma core gases are hot and substrate surfaces are relatively cold. In this
region, thermal diffusion is expected to be important. This situation is fortuituous
since the silicon particles nucleated in the gas phase, because of their higher
density compared to the reactor ambient gases, will move to the substrate
surfaces due to the thermophoretic force, become incorporated, and contribute
to silicon film growth. Srivastava et al. (14) have given a good description
of the particle transport properties and models in silicon deposition systems.

Apart from the transport of particles, transport of other species to and
away from the substrate surface is another important factor that determines
efficiency of the overall deposition system. For example in the simple
reaction*

$$SiCl_4 + H_2 \rightarrow Si(S) + HCl$$

---
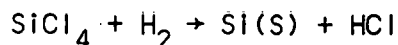
*The actual reaction producing free silicon is known to involve an intermediate
$SiCl_2$ species.

producing free silicon on the substrate surface, $SiCl_4$ has to be transported from the bulk gas stream to the substrate and HCl has to be transported from the substrate to the bulk gas stream. In the systems (or regions of systems) where the substrate is hotter than the bulk gas stream, diffusion of $SiCl_4$ will be retarded while that of HCl will be accelerated. As a result, the substrate sees a lower chlorosilane concentration than the input value. Hence, the observed deposition efficiencies will be higher than predicted by equilibrium calculations, even with CVD.

In this discussion we have only attempted to present various factors that are important in HPP deposition. The qualitative and simplistic description of the HPP process discussed above appears to explain some of the experimental results. However further analysis is necessary to develop a quantitative HPP deposition model.

2.2.5   CHOICE OF SILICON SOURCE GAS

Table 3 compares various chlorosilanes as source gases for silicon deposition by HPP. Silicon tetrachloride is the cheapest and SiH_4 is the most expensive of the gases being considered. However, there is a potential for future reductions in price for $SiHCl_3$, SiH_2Cl_2, and SiH_4 through implementation of advanced technologies currently being developed. Due to an unfavorable market supply and demand situation for semiconductor grade $SiCl_4$, it is currently under priced and it is expected to continue to be so, at least for the next 5 - 10 years. (Semiconductor grade $SiCl_4$ is a biproduct of present polysilicon manufacturing plants.)

As seen in previous sections, the HPP mode of deposition improves the performance of $SiCl_4$ and $SiHCl_3$ as silicon source gases. However due to

23

TABLE 3

COMPARISONS BETWEEN VARIOUS CHLOROSILANES

CHLOROSILANE	TODAYS PRICE		POTENTIAL FOR FUTURE PRICE REDUCTIONS	BENEFIT FROM PLASMA DEPOSITION	SIMPLICITY OF DEPOSITION PROCESS
	$/KG	$/Kg of SI			
$SiCl_4$	0.40	2.43	?	YES	YES
$SiHCl_3$	1.60	7.69	YES	YES	YES
SiH_2Cl_2	56.00	202.00	YES	?	?
SiH_4	400.00	475.00	YES	NO	NO

the low activation energy required for deposition using SiH_2Cl_2 and SiH_4 sources, benefits from HPP are not expected to be significant, particularly when compared to the additional complexity of the HPP process. Furthermore, deposition using SiH_4 as a source gas is expected (known) to be extremely difficult due to severe gas phase nucleation problems. Based on these considerations $SiCl_4$ and $SiHCl_3$ are believed to be more suitable source gases for silicon deposition. The reactor throughput rate will be about a factor of two or more when using $SiHCl_3$ than when using $SiCl_4$. This makes use of $SiHCl_3$ more desirable. However, when using $SiCl_4$, the reactor effluent gas stream contains a significant percentage of $SiHCl_3$, and when this is recovered and recycled, use of $SiCl_4$ as make up appears to be a more economical approach when the low price of $SiCl_4$ is considered.

Problems associated with operation of the present semicontinuous plasma deposition system (employing gas curtains) were discussed in the previous quarterly report. Apart from these operational problems during film deposition, another problem with this approach has been found to be associated with the use of gas curtains. Nitrogen is used in these gas curtains because of its low-cost and compatibility with the silicon deposition process. However N_2 in the deposition reactor effluent will deteriously affect the performance of the recovery process. While argon is suitable (in view of its compatibility with silicon deposition and effluent recovery), it is probibitively expensive.

To overcome all the above difficulties, we have identified a new continuous silicon film deposition scheme that does not utilize gas curtains. The new scheme, a conceptual drawing of which is shown in Figure 10, uses gas interlocks. In this system, a cassette containing a finite number of TESS substrates will be fed into the gas interlock at the entrance side of the reactor, the interlock purged, the cassette moved into the main chamber, the substrates from the cassette translated through the deposition system, and the empty cassette withdrawn from another interlock. By a similar scheme the substrates and separated silicon films are withdrawn from the deposition system. By proper sequencing of these operations, this process will be truly continuous. Nitrogen and hydrogen will be used in proper sequence to purge the gas interlocks so that N_2 is not introduced into the deposition system when the interlock is activated. Apart from differences in the methods of intorducing and withdrawing substrates and separated films, the new process is identical to the presently used one.

A detailed design of this new continuous silicon film deposition system has been initiated, and it should be completed before the end of the next quarter. All four walls of the reaction chamber will be active to produce

CONTINUAL POLYRIBBON FORMATION SYSTEM

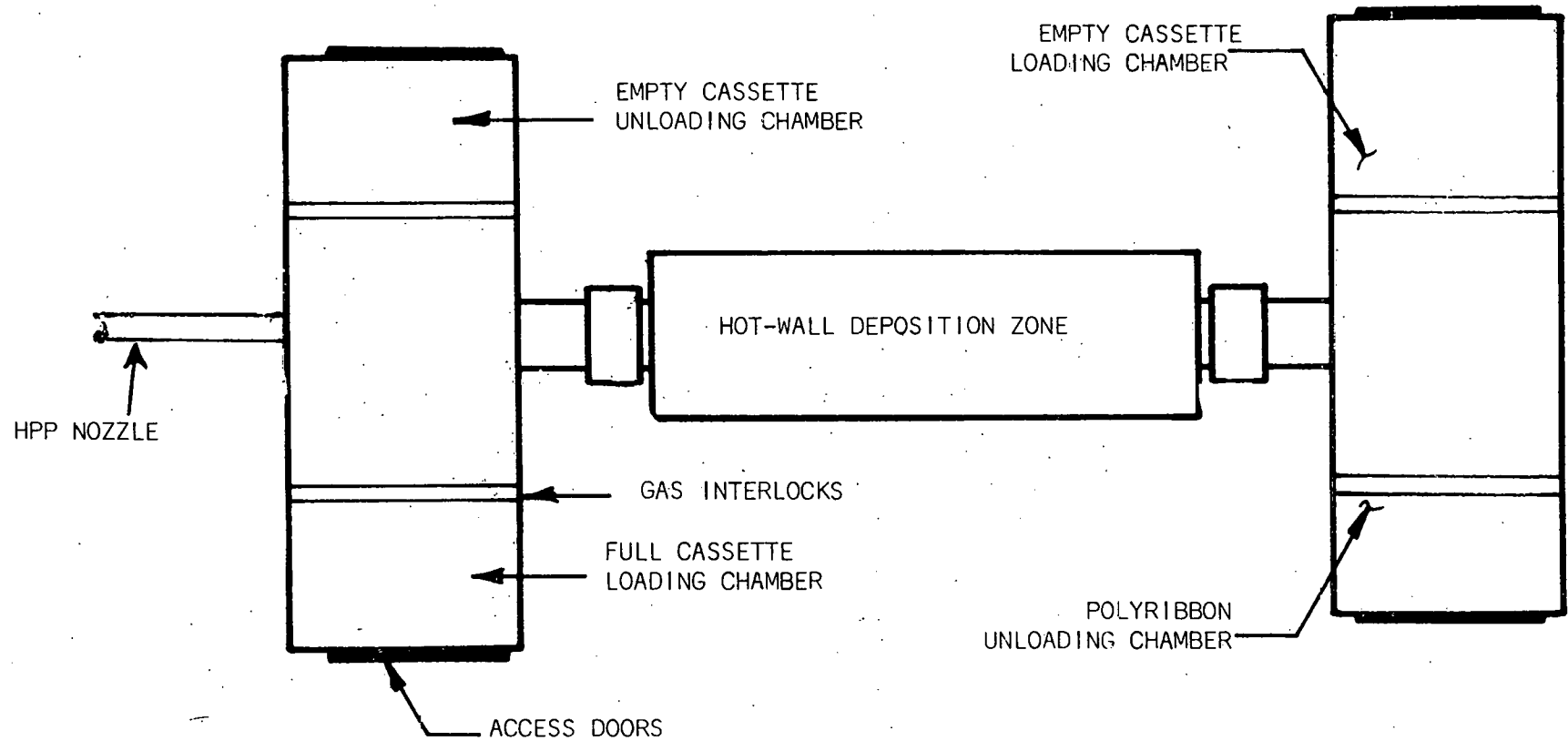FIGURE 10: SCHEMATIC CONCEPTUAL DRAWING OF THE NEW CONTINUAL MICROCRYSTALLINE SILICON DEPOSITION SYSTEM EMPLOYING GAS INTERLOCKS.

four silicon films simultaneously. Silicon film (substrate) size has been selected to be about 7.5 xm x 34 cm for the system design. While this system is being designed and built, we will continue to use the present semicontinuous system for producing microcrystalline silicon films.

4.0   GRAIN SIZE ENHANCEMENT

Although not a part of the current program, some Ribbon-to-Ribbon (RTR) laser recrystallization developments, for the sake of continuity of this report will be beiefly described. Progress has been made in two important areas: 1) development of imporved pre- and post-heaters and 2) development of a new feed mechanism. The new pre- and post-heaters were constructed from Si C elements (replacing the previous platinum helements). Performance of these new heaters is found to be much superior to the old ones in terms of improved thermal profiles in the ribbon and lower heater down times. The new feed mechanism is more versatile and allows grain enhancement from one end of the ribbon to the other.

Several silicon material quality related experiments were performed, by using a variety of feedstock materials for laser recrystallization. The results of these experiments are discussed in the next section.

5.0   SOLAR CELL FABRICATION AND EVALUATION

In the present quarter, three separate but interrelated solar cell fabrication experiments were completed. They are described in detail in the following three subsections. The first experiment consists of "standard RTR growth" and a baseline solar cell process sequence applied to ribbons grown from high purity, oxygen-free, single crystal float zone silicon. This experiment is designed to assess the solar cell potential of RTR silicon independent of possible feedstock contamination.

The second experiment consists of solar cell fabrication on ribbons grown from CVD microcrystalline feedstock. Two resistivities of the p-type feedstock were used, and the effect of resistivity on efficiency is discussed.

The third group of solar cells fabricated are on ribbons grown from high pressure plasma deposited microcrystalline feedstock deposited in the semicontinuous (gas curtain) apparatus.

The baseline solar cell process sequence used for all three groups consisted of:

PH_3 diffusion - 18 min, $900^{\circ}C$

Mesa Pattern Definition and Etch - Photolithography and CF_4 (92%) -
   O_2 (8%) plasma etching.

Si_3N_4 AR Coating - LPCVD, $850\overset{\circ}{A}$, index of refraction = 2.0

Metallization pattern definition and etch - Photolithography, CF_4 (50%) -
   O_2 (50%) plasma etching.

Plated metal - Pd-Ni-Cu

This sequence uses a metallization pattern which has not been fully optimized to minimize both series resistance and the percentage of shadowing. As a result, the fill factor is reduced by a factor of from 2 to 5% for the samples with short circuit current densities $\geq$ 26 mA/cm^2. Also, with the exception of several samples of HPP orign as noted later, no texture etching of the illuminated surface was done.

Feedstock for RTR silicon ribbon growth was obtained by sawing a float zone silicon ingot into sheets with an area of 1.15" x 7.5" and with a thickness of 10 ± 1 mils, and etching to remove the saw damaged surfaces.

This single crystal material was recrystallized in the RTR apparatus, and the processed into solar cells using the baseline process sequence along with unmelted control samples. The recrystallized ribbons differed from grain-enhanced HPP ribbons in two ways; 1) because of the quality of the starting material, any possible contamination from molybdenum, or from fast diffusing impurities in the molybdenum, or from the deposition furnace, are eliminated from consdieration, and 2) because the starting material was single crystal, the regrown ribbons retained the single crystallinity in some cases. The ribbons that did not retain the single crystallinity were characterized by the presence of multiple twin planes very similar to the ones in grain enhanced HPP ribbons. Table 4 summarizes the results obtained.

It can be seen from Table 4 that when single crystallinity is maintained after RTR growth, solar cell performance is scarcely different from the control cell on float zone feedstock. Thus, chemical contamination during RTR growth (from the growth chamber, pre-heater and post-heater) appears to be inconsequential. The RTR single crystal cell, however was found to contain higher dislocation density ($7 \times 10^4/cm^2$) compared to the float zone single crystal control cell.

5.2   SOLAR CELLS ON RTR SILICON GROWN FROM CVD FEEDSTOCK

Ribbons grown from CVD microcrystalline feedstock were divided into two groups; a low resistivity (~0.30 Ω-cm lot) and a moderate resistivity lot (~ 2.4 Ω-cm). The results on solar cells fabricated by the baseline process

TABLE 4

SUMMARY OF RESULTS OBTAINED USING FLOAT ZONE SILICON FEEDSTOCK.

SOLAR CELL DESCRIPTION	AM1 EFFICIENCY (%)	J_{SC} (mA/cm^2)	V_{OC} (volts)
Float Zone Single Crystal Control	14.8	32.3	.606
RTR Single Crystal (Float Zone Feedstock)	14.5	31.4	.601
RTR Heavily Twinned (Float Zone Feedstock)	13.0	30.7	.586
Best RTR Cell-Oxygen Free, CVD Feedstock	12.8	27.5	.608

sequence are presented in table 5. The loss in J_{SC} due to doping effects on diffusion length, as resistivity is lowered, is more than made up for by the increase in V_{OC}. The difference in fill factor between the two lots is small, and is partially an artifact of the non-optimum grid design used. The metallization pattern used provides the optimal tradeoff between shadowing of the junction and resistive losses for cells having short circuit currents of up to 26 mA/cm^2. Since these cells average better than this, the fill factor is reduced from what a better pattern could provide, and the effect (i.e. amount of reduction) will be slightly greater for the 2.4 Ω-cm lot. An estimate of the quantitative effect of this grid design on fill factor was obtained for one cell (1185A-4B, with V_{OC} = .608, J_{SC} = 27.5 mA/cm^2, and F.F. = 77.0%) by numerically fitting the i-v characteristics and subtracting the effect of a constant, lumped series resistance. This allowed for the calculation of a "semiempirical" fill factor, which in this case worked out to be 80.1%. This represents an upper limit dictated entirely by the short circuit current and the junction i-v properties. An optimal grid design can be expected to increase the actual fill factor 1 - 2 percentage points.

Another cell (with η = 11.9%) from the low resistivity lot was given a 6 min. Wright etch to delineate dislocations. The results for a front surface etch are shown in Figure 11 and for a cross section in Figure 12. These results are typical of present day RTR silicon (grown from microcrystalline feedstock), and appear to be improvable by further work on the post-heater thermal profile. It is somewhat surprising (and encouraging) that solar cells with efficiencies of 12 - 13% can be made on material having regions with high ($\geq 1 \times 10^6$/cm^2) dislocation density.

TABLE 5

RTR SOLAR CELL PERFORMANCE FROM CVD FEEDSTOCK

RESISTIVITY Ω-cm	AM1 EFFICIENCY (%)		J_{SC} (mA/cm^2)		V_{OC} (volts)		F.F. (%)	
	AVE.	MAX*	AVE.	MAX*	AVE.	MAX*	AVE.	MAX*
2.4	11.04	12.2	29.0	30.9	0.521	0.537	73.0	75.8
0.3	11.65	12.8	26.43	29.3	0.595	0.608	74.2	78.8

*Maximum values not obtained simultaneously.
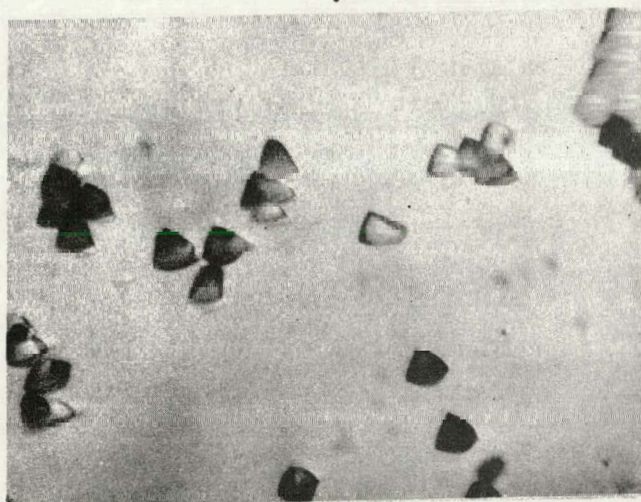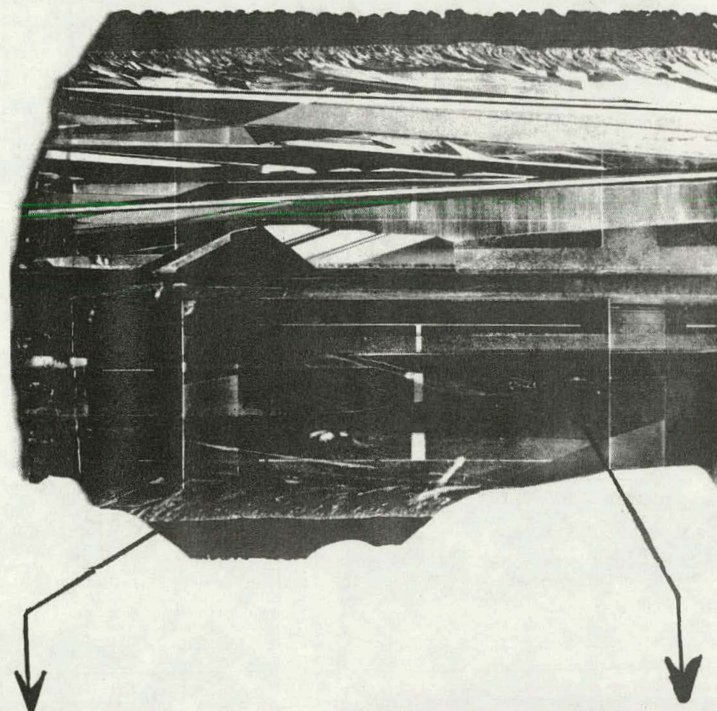
Dislocation Density = $5 \times 10^5/cm^2$ Dislocation Density = $1 \times 10^6/cm^2$

FIGURE 11:   DISLOCATION ETCH PITS ON THE SURFACE OF A CELL AS
             REVEALED BY 6 MINUTES   WRIGHT ETCHING.
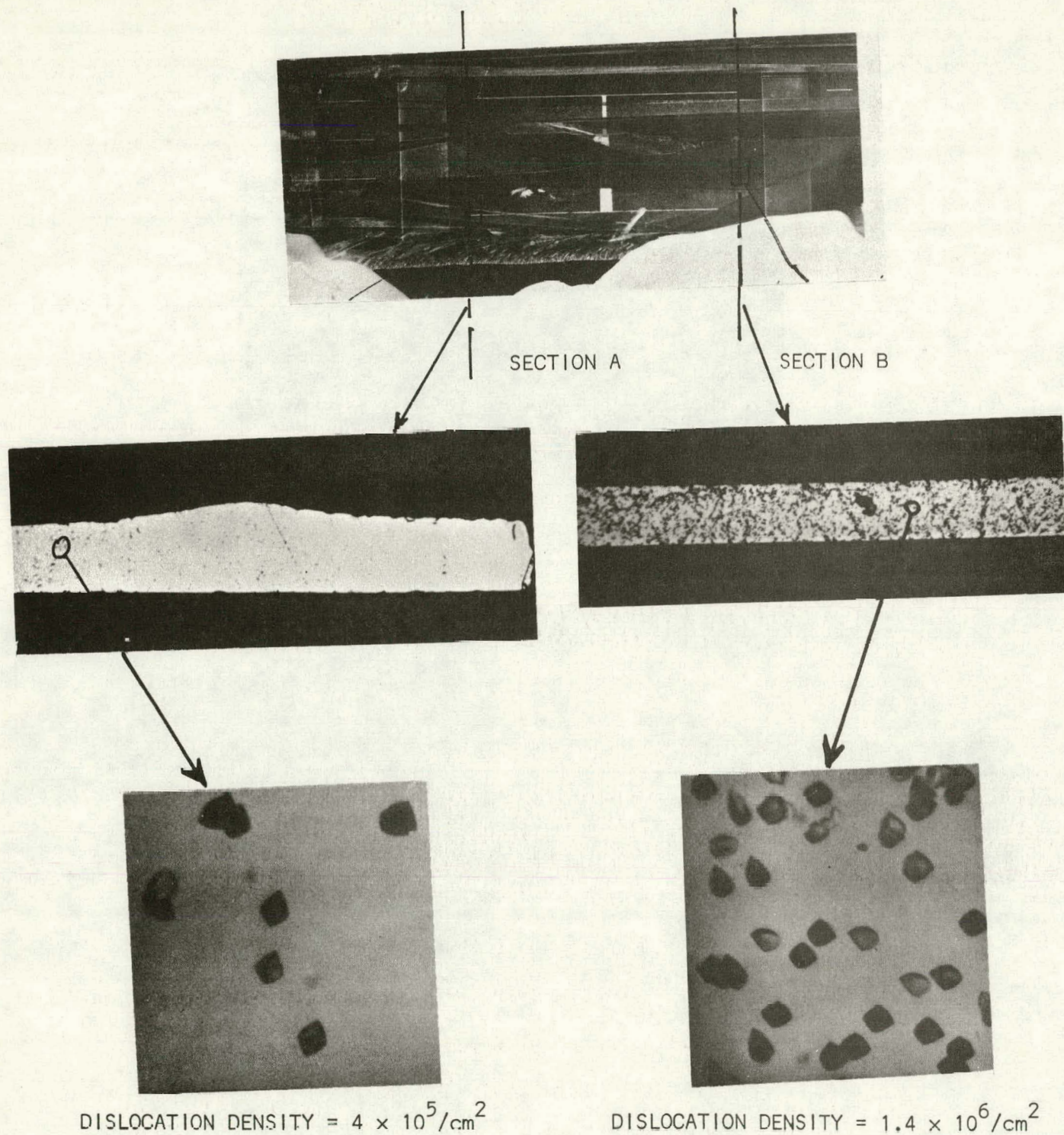
DISLOCATION DENSITY = $4 \times 10^5/cm^2$ DISLOCATION DENSITY = $1.4 \times 10^6/cm^2$

FIGURE 12:   DISLOCATION DENSITY IN THE BULK OF THE CELL SHOWN
IN FIGURE 11, AS REVEALED BY WRIGHT ETCHING THE
CROSS SECTIONAL SAMPLES.

5.3   SOLAR CELLS FROM GRAIN ENHANCED HPP SILICON FILMS

Results on typical solar cells fabricated on grain enhanced HPP films are summarized in Table 6. Unlike the cells fabricated on RTR rpocessed float zone or CVD feedstock reported in the previous sections, some of the HPP cells were larger in size (2 cm x 2 cm). Also some of these cells were fabricated on textured surfaces (to minimize front surface reflection) as indicated in Table 6. Another difference between the float zone feedstock and HPP feedstock is the silicon thickness; thickness of HPP feedstock was around 175 μm, whereas that of float zone was around 250 μm.

The highest efficiency observed in this lot was about 12%, and was on 2 cm x 2 cm area textured cell shown in Figure 13. The other parameters of this cell are: V_{OC} = 0.582 volts, J_{SC} = 28.3 mA/cm^2 and F.F. = 73.0%. The defect structure of these grain enhanced HPP films is similar to the ones reported in the previous quarterly report (12), since the same recrystallization parameters were employed.

Comparing the results obtained with the float zone, CVD and, HPP silicon ribbons, it appears that the major factor limiting the performance of the HPP or CVD films is the defect density of the grain enhanced films, and not the chemical purity of the feedstock material. Thus, when the defect density (dislocations, incoherent twin boundaries and grain boundaries) is reduced by optimization of RTR grain enhancement growth parameters, further improvements in solar cell conversion efficiency can be expected.

TABLE 6

SUMMARY OF TYPICAL SOLAR CELLS FROM GRAIN ENHANCED HPP DEPOSITED FILMS

| CELL I.D.		CELL SIZE	V_{OC}	J_{SC}	F.F.	η (AM1)	COMMENTS
HPP	RTR	(cm × cm)	(volts)	(mA/cm^2)	(%)	(%)	
13-9	1201C-1	1 X 2	0.541	23.0	71.5	8.9	Non-textured
	-2	1 X 2	0.559	25.0	70.8	9.9	"
	-3	1 X 2	0.561	25.0	72.7	10.2	"
17-4	1201G-1	2 X 2	0.579	25.6	75.6	11.2	Textured
	-2	2 X 2	0.582	26.0	74.5	11.3	"
	-3	2 X 2	0.580	26.3	70.4	10.7	"
18-4	1201B-1	1 X 2	0.577	25.8	74.6	11.1	Non-textured
	-2	1 X 2	0.575	24.5	71.0	10.0	"
18-6	1201E-1	2 X 2	0.582	28.3	73.0	12.0	Textured
21-6	1219A-1	2 X 2	0.573	26.7	73.9	11.3	"
	-2	2 X 2	0.570	26.5	69.5	10.5	"
	-3	1 X 2	0.558	25.5	69.6	9.9	"
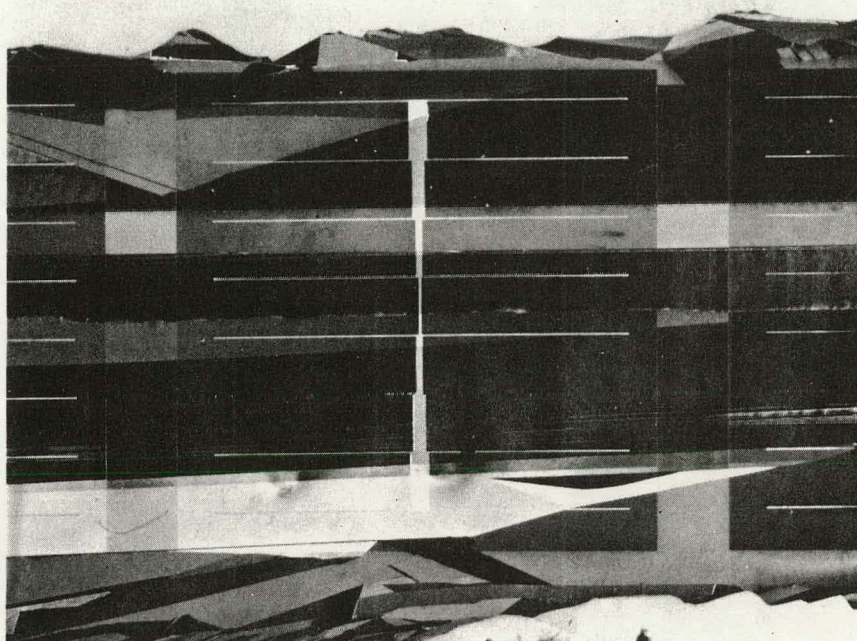
FIGURE 13:   PHOTOGRAPH OF A 12% AM1 EFFICIENCY
(2 cm × 2 cm AREA) CELL FABRICATED ON
A GRAIN ENHANCED HPP DEPOSITED SILICON
FILM. V_{OC} = 0.582V, J_{SC} = 28.3 mA/cm^2
and FF = 73.0%.

During the next quarter we plan to:

. Continue periodic TESS substrate resurfacing experiments.

. Complete design of the continuous silicon film deposition system employing gas interlocks.

. Continue operation of the existing semicontinuous plasma deposition system, and

. Demonstrate > 12% AM1 conversion efficiency on > 10 cm^2 area solar cells fabricated on grain enhanced plasma deposited silicon films.

REFERENCES

1. K. R. Sarma, et al., Thin Film Polycrystalline Silicon Solar Cells, Quarterly Report 1, Dec. 1979, DOE Contract No: XS-9-8277-1.

2. K. R. Sarma et al., Thin Film Polycrystalline Silicon Solar Cells, Quarterly Report 2, March 1980, DOE Contract No. XS-9-8277-1.

3. C. W. Monke and L. F. Donaghey, J. Electrochem. Soc., 124, 561 (1977).

4. K. R. Sarma et al., Thin Films of Silicon on Low-Cost Substrates, Final Report, Sept. 1978, DOE Contract No. EY-76-C-03-1287.

5. K. R. Sarma et al., In Proc. 13th IEEE Photovoltaic Specialists Conference, pp 466, June 1978, Washington D.C.

6. L. P. Hunt et al., Proc. 2nd International Conference on Chemical Vapor Deposition, pp. 3 - 24, 1969.

7. E. Sirtl et al., J. Electrochem. Soc., 121, 925 (1974).

8. L. P. Hunt et al., J. Electrochem. Soc., 119, 1741 (1972).

9. JANAF Thermo Chemical Tables, Ed. D. R. Stull, Constantly updated.

10. F. C. Eversteijn, Philips Research Reports, 26, 134 (1971).

11. T.U.M.S. Murthy et al., J. Crystal Growth, 33, 1 (1976).

12. K. J. Sladek, J. Electrochem. Soc., 118, 654 (1971).

13. K. R. Sarma et al., Thin Film Polycrystalline Silicon Solar Cells, Annual Report, Sept. 1979, DOE Contract No. ET-78-C-03-2207.

14. R. Srivastava and R. K. Gould, Development of a Model and Computer Code to Describe Solar Grade Silicon Production Processes, 7th Quarterly Report, August 1979, DOE/JPL 954862-79/7.